JOURNAL OF MAGNETIC RESONANCE, Series A 103, 13–22 (1993)

Rapid Quantitation of Parameters from Inhomogeneously Broadened EPR Spectra

HOWARD J. HALPERN,* MIROSLAV PERIC,*†‡ CHENG YU,* AND BARNEY L. BALES§

*Michael Reese/University of Chicago Center for Radiation Therapy and the Department of Radiation & Cellular Oncology, University of Chicago, Chicago, Illinois 60637; and §Department of Physics & Astronomy, California State University, Northridge, California 91330

Received April 30, 1992; revised September 28, 1992

Spectral parameters from inhomogeneously broadened organic-free-radical EPR spectra, using nearly all the information in the spectrum, were extracted rapidly and accurately using an approximation of the spectral shape by the *sum* of a Lorentzian and a Gaussian function of equal linewidths. This approximate shape was fitted to the spectrum by a nonlinear least-squares fitting algorithm. Line position and overall spectral width were extracted directly, whereas component Lorentzian and Gaussian widths were extracted with further analysis of the fit parameters. We investigated the accuracy with which the sum function can be fitted to the more familiar Lorentzian/Gaussian convolution (Voigt) representation of EPR spectra for both a singlet and a closely spaced (overlapping) doublet spectrum. The strategy was applied, first, to synthetic spectra involving noise added to the Voigt doublet and, second, to spectral data from a nitroxide manifold consisting of a closely spaced doublet. This parametric extraction strategy increased the accuracy of the line-splitting measurement by an order of magnitude compared with other methods. It allowed deconvolution of the component Lorentzian linewidth that is consistent with previous direct measurements. It may allow the probing of subtle physical variations which have heretofore been difficult, if not impossible, to measure.

INTRODUCTION

This paper describes a fast and accurate fitting algorithm for spectral lines subject to both inhomogeneous and homogeneous broadening. A commonly used representation (*1, 2*) of an inhomogeneously broadened lineshape is a convolution of the Lorentzian spin-packet form with a Gaussian approximation to the binomial (or multinomial) weight of the unresolved spectral lines. The derivative of this convolution will be referred to as the Voigt or Voigt profile (*1*). The computation time involved in the evaluation of this convolution has discouraged its wide use in fitting, in which multiple iterations may be necessary for adequate fits. However, it is well known that the Voigt is well represented by a function that is the *sum* of a Gaussian function and a Lorentzian function, for both absorption (*3*) and first-derivative line profiles [(*4*) and early Varian EPR manuals]. In this paper, all references to spectral lines imply first-derivative lines unless otherwise specified.

The sum of derivative Gaussian and Lorentzian functions—referred to as the sum function—may be evaluated quite rapidly and [(*4*), vide infra] with excellent approximation to the Voigt. The previous context in which this functional form was presented (*4–6*) presumed an excellent signal-to-noise ratio, in which case a few representative points of the spectrum were sufficient for reliable extraction of the physically relevant parameters of the lineshape. The extraction of spectral parameters with the use of only a few points of the spectrum ignores the information in the spectrum not included in the immediate region of these points. Under conditions of high noise or sample instability (e.g., those involved with measurements from a living animal), it may be necessary to bring the information of the full spectrum to bear on the extraction of spectral parameters. This can be done with spectral fitting.

We describe the adequacy with which two formulations of the sum function can fit both a Voigt function form and spectral data. The formulations differ in their normalization—one is normalized to unit peak-to-peak amplitude, and the other is normalized to unit area. The sum functions were first fitted to a singlet Voigt line. The deviation of the spectral parameters of the Voigt from those of the sum functions depends on the region over which the spectrum is fitted. Next, the sum function was used for extraction of spectral-shape parameters of a doublet of Voigt lines with line splitting equal to 1.5 peak-to-peak linewidths. We also investigated the effect of noise added to the spectrum.

Finally, the technique was applied to the quantitative extraction of the physical variables measured in the EPR spectrum of a nitroxide designed to optimize spin-label oximetry. This example presents a system of substantial complexity—an overlapping doublet each of whose lines consists of the same inhomogeneous and homogeneous components. From

† Current address: Department of Astronomy and Physics, California State University at Northridge, Northridge, California 91330.

‡ On leave of absence from Ruder Boskovic Institute, Zagreb, Croatia.

1064-1858/93 $5.00

this system, spectral fits and quantitative spectral information were derived, and inhomogeneous and homogeneous lineshape components were measured. Comparisons with direct measurements of the homogeneous lineshape parameters validate the method.

BACKGROUND

Inhomogeneously broadened EPR spectra can be described with both good fidelity and good justification by the derivative of the normalized convolution of Lorentzian and Gaussian functions, or the Voigt function, provided that the inhomogeneous, or Gaussian, component of the linewidth is not too large. Following the conventions of Bales (*4*), this convolution can be reduced to a functional form, the *shape* of which can be characterized by a single parameter, χ_{Voigt}, as

$$F(B) = -K\frac{(2)^{3/2}}{3^{1/2}\pi^{3/2}(\Delta B_{pp}^{G})^{3}\Delta B_{pp}^{L}} \times \int_{-\infty}^{\infty}\frac{4(B'-B_0)\exp\{-2[(B'-B_0)/\Delta B_{pp}^{G}]^2\}}{1+(4/3)[(B-B')/\Delta B_{pp}^{L}]^2}\,dB' \quad [1]$$

$$= F[B(u)] = F(u) \quad [2]$$

$$= -K\frac{2^{3/2}\chi_{Voigt}}{3^{1/2}\pi^{3/2}(\Delta B_{pp}^{G})^2}\int_{-\infty}^{\infty}\frac{2v\exp(-v^2)dv}{1+2\chi_{Voigt}^2(u-v)^2/3}$$

$$\chi_{Voigt} \equiv \Delta B_{pp}^{G}/\Delta B_{pp}^{L}. \quad [3]$$

Here, ΔB_{pp}^{L} is the Lorentzian peak-to-peak linewidth, ΔB_{pp}^{G} is the Gaussian peak-to-peak linewidth, and B_0 is the center of the line. K is equal to the doubly integrated intensity or the area of the absorption line; χ_{Voigt} is proportional to the parameter p used by Zemansky (*7*) and to the parameter a of Castner (*8*) and Poesner (*9*), and

$$u = (2)^{1/2}(B-B_0)/\Delta B_{pp}^{G} \quad [4a]$$

$$v = (2)^{1/2}(B'-B_0)/\Delta B_{pp}^{G}. \quad [4b]$$

The nonderivative convolution of the Gaussian and Lorentzian is approximated to 0.7% by a variably weighted sum of Gaussian and Lorentzian terms of equal peak-to-peak linewidth (*3*). The derivative spectral form presented above can be approximated to 0.5% (*10*) by the variably weighted sum of the derivatives of the Gaussian and Lorentzian functions of equal peak-to-peak linewidth. This sum can be described by two forms which differ in their normalizations: F_H is normalized to unit peak-to-peak amplitude (V_{pp}), and F_A is normalized to unit doubly integrated intensity (A) (*4*):

$$F_H[B(x)] = -V_{pp}\left[\eta_H\frac{8x}{(3+x^2)^2} + (1-\eta_H)\frac{e^{1/2}x}{2}\exp\left(-\frac{x^2}{2}\right)\right] \quad [5]$$

$$F_A[B(x)] = -A\left[\eta_A\frac{8\sqrt{3}}{\pi(\Delta B_{pp}^{0})^2}\frac{x}{(3+x^2)^2} + (1-\eta_A)\frac{4x}{\sqrt{2\pi}(\Delta B_{pp}^{0})^2}\exp\left(-\frac{X^2}{2}\right)\right]. \quad [6]$$

For $V_{pp} = 1$, the peak-to-peak signal amplitude of the derivative sum function is unity, independent of η_H. For $A = 1$, the doubly integrated intensity is unity, independent of η_A:

$$x = 2(B-B_0)/\Delta B_{pp}^{0}. \quad [7]$$

B_0 is the center of the line, ΔB_{pp}^{0} is the peak-to-peak linewidth common to both the derivative Gaussian and the Lorentzian components of both sum functions, and η_H and η_A is a normalized, variable-weight term for F_H or F_A, respectively. Simple linear transformations which relate the weights of the two functional forms appear in the Appendix.

The sum-function spectral shape is determined by a single parameter, η_A or η_H ($=\eta$), as recognized by Wertheim *et al.* (*3*). Because the Voigt function is dependent on a single parameter, χ_{Voigt}, a transformation can be established between η and χ_{Voigt}. Thus, should information concerning the Gaussian and Lorentzian component linewidths be desired, fits of data to the sum function can be performed rapidly, and the overall linewidth ΔB_{pp}^{0} and the sum-function weight term η_H or η_A can be extracted and transformed to the convolution parameter χ_{Voigt}.

A useful form of the transformation from η to χ_{Voigt} is

$$\chi_{Voigt} = \frac{a\eta^2 + b\eta + c}{\eta^2 + d\eta + e}. \quad [8]$$

The separate Gaussian and Lorentzian widths of the convolution can be derived from η and ΔB_{pp}^{0} of the sum function as follows. The χ_{Voigt} can be obtained from [8]. Then, from the relationships of Dobryakov and Lebdev, which are accurate to 0.5% (*4, 10*),

$$\Delta B_{pp}^{L} = \Delta B_{pp}^{0}\frac{(1+4\chi_{Voigt}^2)^{1/2}-1}{2\chi_{Voigt}^2} \quad [9a]$$

$$\Delta B_{pp}^{G} = \chi_{Voigt}\Delta B_{pp}^{L}. \quad [9b]$$

MATERIALS AND METHODS

Fitting Strategy

The basic strategy of this approach is fourfold: (1) Derive a rapidly evaluable analytic functional form with variable

parameters, some of which may have *no* particular physical basis. Within the likely range of variation of its parameters, the functional form *must* fit the actual spectrum well. The functional form chosen, as discussed above, consists of a single line or of two lines, each of which is the sum of Lorentzian and Gaussian functions. (2) Use this function to fit a relatively complex spectrum by employing a nonlinear least-squares fitting algorithm. (3) Relate the fit parameters to physically relevant parameters by means of a predetermined map. (4) Extract statistical uncertainties in the fit parameters due to spectral noise.

The goodness-of-fit criterion was the χ^2. The use of an analytical functional form, in Eq. [5] or [6], to fit the spectrum allowed the use of parameter gradient information. The Levenberg–Marquardt algorithm provided rapid convergence to global minima provided that reasonably good test functions and initial parameters were selected. This algorithm is well known and available (*11*) and allowed a rapid estimate of uncertainties in fit parameters.

For all fits to be described, initial linewidths, line heights, and line positions were generated by searching for crude local maxima and minima in the input data. The initial sum-weight parameter η was set equal to 0.5. The initial linear baseline, where applicable (i.e., with spectral data), was determined by averaging of the first and last 5% of the spectral data points.

The adequacy of the parameters extracted from the sum function relative to those of the Voigt was estimated by treatment of points of the Voigt (Eq. [2]) as synthetic data and fitting the sum function to them. A χ_{Voigt} and an initial linewidth were chosen. The Gaussian and Lorentzian linewidths were evaluated from Eq. [9] and assigned to be the exact values of these parameters. The "exact" peak-to-peak linewidth of the Voigt with these component linewidths was evaluated numerically from the full Voigt integral. The exact Voigt linewidth was then compared to ΔB^0_{pp}, which was assigned to the sum function by the fitting procedure. This procedure allows the variation of the input χ_{Voigt} over a relatively large range while maintaining the linewidth constant to within 0.5%.

The Voigt doublet was modeled as the sum of two derivative convolution functions with the peak-to-peak linewidth multiples of the line splitting ranging from 2/3 to 4. This modeling focused on a peak-to-peak linewidth/splitting ratio of 2/3 or a full-width-at-half-maximum/splitting ratio of ~ 1. This corresponds to the mean overall linewidth/splitting ratio of the nitroxide spectral data to be discussed. Each Voigt line was assumed to have the same height and Lorentzian and Gaussian components. The two sum functions that were fitted to this doublet were constrained to have identical line parameters (common width ΔB^0_{pp}, spectral amplitude, and Lorentzian/Gaussian weight η) except for the line positions that define the splitting.

For some measurements, random noise was added to the Voigt doublet profile. One hundred sets of Gaussian noise (*12*) were generated of standard deviation (σ) equal to 2.5% of the V_{pp} and added to the Voigt. The sum function was then fitted to each of the resulting spectra.

Sample Preparation and Spectral Acquisition Conditions

The compound 4-hydro-3-carbamoyltetraperdeuteromethyl-3-pyrrolinyl-1-oxy, mHCTPO (*13, 14*), has collapsed methyl splittings via the deuterium substitutions. The ring hydrogen is retained. This induces a splitting of approximately 500 mG which varies with spin-label concentration (but not with dissolved oxygen concentration) (*13*), temperature, and solvent (*15*). The linewidth, which varies with the spin-label concentration and oxygen concentration (*13*), varied from 280 to 500 mG under the conditions described. The compound synthesis has been described previously (*14*). We estimate the contamination of the ring hydrogen with deuterium to have been 2%. Samples were measured at room temperature (27°C).

Spectra were measured at 250 MHz (*16*). This low frequency was chosen for measurements to be made in the tissues of a living animal. There is little change in the aqueous spectra relative to those at X band (*16, 17*). A low magnetic field ($g = 2$ is $\sim$90 G) gives good stability. Samples of mHCTPO were prepared as 10 ml, 0.05 to 1.0 m*M* aqueous solutions. Oxygen concentrations varied from less than 1 to 268 μM. The radiofrequency power was 1 mW ($B_1 \sim 40$ mG), the modulation amplitude was 0.1 G, the modulation frequency was 5.12 kHz, the time constant was 0.1 s, and the data point acquisition time was 0.1 s, with 256 points per scan, 10 scans per spectrum. The spectral field window encompassed at least four individual linewidths of the central nitrogen manifold doublet plus the doublet splitting.

Sum Function for Fitting of Nitroxide Spectra

The function to which the nitroxide spectra were fitted consisted of a pair of Gaussian/Lorentzian sum functions constrained to have identical amplitudes, common linewidths ΔB^0_{pp}, and Lorentzian weights η. A linear baseline term was included in the fitting function. A third line, the amplitude of which was 4% that of the amplitude of each doublet line and the width of which was fixed to be 16% larger than that of the doublet linewidth, was added to the fitting function and centered between the doublet lines. This represents contamination of the mHCTPO with perdeuterated CTPO.[1] From the η–χ_{Voigt} transformation for the Voigt

[1] Early syntheses of the mHCTPO compound showed constant deviations of the fitting function from spectra of the central nitrogen doublet manifold. Residuals indicated a third line, centered between the doublet line, consistent with approximately a 15% perdeuterate contamination. Prolonging the exchange step in the synthesis of the mHCTPO reduced the contamination to 2%.

doublet with a fit region of four linewidths and from Eqs. [9a] and [9b], Lorentzian and Gaussian linewidths were extracted from the doublet spectra.

Uncertainty Estimates in the Parameters from Fits to Nitroxide Spectra

Variance estimates in the parameters extracted from the fits were obtained by multiplication of the diagonal elements of the covariance matrix generated by the Levenberg–Marquardt algorithm (the "error" matrix) by the χ^2 per degree of freedom in the standard fashion (*18, 19*). Residuals indicated that there was no systematic deviation of the fit from the data. Histograms of the residuals were consistent with a Gaussian distribution (data not shown). Estimates of uncertainties of dependent parameters (e.g., ΔB_{pp}^{L} in Eqs. [8] and [9]) were propagated in the standard fashion, assuming, for simplicity, that parameters extracted directly from the fit were uncorrelated (*20*).

In fits to hypotheses thought to reflect the behavior of the spectral parameters, weights were assigned to each data point that were equal to the inverse of the variance (*21*). A simpler hypothesis governing the behavior of the data was chosen over a more complicated hypothesis when the more complicated hypothesis failed to reduce the χ^2 per degree of freedom of the fit by more than 30%. Variance in fit parameters of the hypothesis was evaluated with variable point weighting.

RESULTS

Fitting Spectral Simulations

Both of the sum functions fitted the derivative singlet Voigt to within at most 7 parts per thousand. Fit parameters extracted with both normalizations were virtually identical. The capability of both the area- and the height-normalized sum-function fits to extract intrinsic first-derivative spectral parameters was tested by comparison of the overall linewidth, the line center, and the height of the Voigt with those derived from the sum functions. The fidelity of the sum-function fit to the Voigt will depend on χ_{Voigt} and the field (or frequency) interval of the fit. Table 1 shows the percentage deviation of various parameters of the fitted sum function from those of the Voigt. These values are given for the χ_{Voigt} at which the deviation was *maximal*. With optimal fit regions, ΔB_{pp}^{0} and V_{pp} deviated less than 0.2 and 0.6%, with deviations of less than 1% for arbitrarily large fit regions.

TABLE 1

Percentage Deviation of Various Parameters of the Singlet Sum Function from Those of the Singlet Voigt for Various Fit Regions

Parameter	Maximum deviation (χ_{Voigt})	Maximum deviation (χ_{Voigt})	Maximum deviation (χ_{Voigt})
Fit region (linewidths)	3.2	4.0	10.0
Linewidth (%)	0.2 (3)	0.2 (0.5)	0.5 (1)
Height (%)	0.5 (1)	0.6 (1)	0.9 (1)

Note. The fit region is defined in units of peak-to-peak Voigt linewidths. Linewidth refers to the deviation of the fitted overall linewidth of the sum, defined by the fit parameter ΔB_{pp}^{0}, the common Gaussian, and the Lorentzian linewidth used in Eqs. [5] and [6], from the peak-to-peak linewidth of the Voigt. The χ_{Voigt} shown in parentheses is selected from the values 0.25, 0.5, 1.0, and 3.0 at which the parameter deviation was maximum.

TABLE 2

Percentage Deviation of Various Parameters of the Doublet Sum Function from Those of the Doublet Voigt for Various Fit Regions

Parameter	Maximum deviation (χ_{Voigt})	Maximum deviation (χ_{Voigt})	Maximum deviation (χ_{Voigt})
Fit region (linewidths)	3.2	4.0	10.0
Linewidth (%)	0.2 (3)	0.2 (0.5)	0.6 (3)
Height (%)	0.6 (1)	0.6 (1)	1.0 (1)
Splitting (%)	0.3 (1)	0.3 (1)	0.4 (1)
R parameter (%)	0.3 (0.5)	0.3 (1)	0.4 (1)

Note. The fit region is defined in units of the number of peak-to-peak Voigt linewidths plus the doublet splitting. The definition of the sum-function linewidth is as given in the note to Table 1, with the lines of the doublet assumed to have identical width. The linewidth deviation is that of the fitted overall linewidth of each line of the sum-function *doublet* from the exact peak-to-peak linewidth of each line of the Voigt doublet. The R value is defined in the legend to Fig. 1. Fits for which height- (Eq. [5]) and area-normalized functions (Eq. [6]) were used gave identical results. Again, the χ_{Voigt} shown in parentheses is selected from the values 0.25, 0.5, 1.0, and 3.0 at which the parameter deviation was maximum.

The fit to two overlapping lines, primarily a pair with linewidth two-thirds of the splitting, assumed to have identical homogeneous and inhomogeneous components, presents a substantially greater degree of complexity. Again, the fidelity of the fit of the sum function to the Voigt is dependent on the fit region, which is defined as the number of Voigt linewidths plus the line splitting, and χ_{Voigt}. Table 2 shows the percentage deviation of various parameters of the fitted sum-function doublet from the corresponding parameters of the Voigt, for χ_{Voigt} at which the deviation was maximal. Of particular note is the splitting reproducibility, where, for a fit region of four linewidths plus the splitting, a maximum deviation of 0.3% was measured. The R parameter, a doublet spectral-shape parameter defined in the legend to Fig. 1, was reproduced to within 0.3% with this fit region.

It seems clear from the above that fitting should be done in *two passes*. From the first pass, an initial estimate of the linewidth can be obtained. The second pass is performed with fit-region restriction. The extra time which this procedure involves is relatively small in that the first pass provides good initial parameters for the second pass.

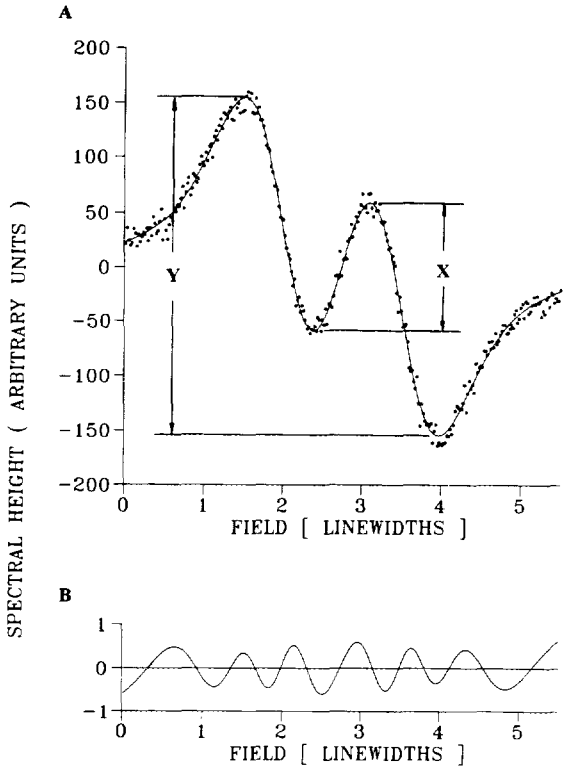

FIG. 1. (A) Voigt doublet (· · ·) to which Gaussian noise of standard deviation σ = 2.5% V_{pp} has been added with doublet sum-function fit (—). The fit region is four peak-to-peak linewidths *plus* the splitting as indicated in the figure. The Voigt doublet linewidth is 2/3 of the splitting. Also shown are the heights of the flanking peak and trough (Y) and the central trough and peak (X). An intrinsic shape parameter, the ratio of these heights designated $R = X/Y$, provides a lineshape measure that is quite sensitive to linewidth and splitting. (B) Residuals of the Voigt *without noise* minus the sum function. The residual scale is the same arbitrary unit as that for the Voigt and sum functions.

The transformation between η and the convolution linewidth ratio χ_{Voigt} was derived from fits of the sum-functional form to Voigt profiles for different input values of χ_{Voigt} that yield corresponding values of η. The (χ_{Voigt}, η) pairs are shown in Fig. 2 for both the doubly integrated intensity- and height-normalized sum functions. Coefficients of the rational function, Eq. [8], are derived by fitting Eq. [8] to the η–χ_{Voigt} pairs for both the area- and the height-normalized sum functions. The coefficients for typical fit regions are enumerated in Table 3. The η determined by the sum-function fit for a particular input χ_{Voigt} varies with the fit region, as indicated by the variation of the coefficients in Table 3. To indicate the effect that the fit region has on the η–χ_{Voigt} transformation, the deviation of the χ_{Voigt} at a given η for various fit regions from those calculated for a fit region of four linewidths is shown as a function of χ_{Voigt} in the insert to Fig. 2. As with the singlet, the doublet η–χ_{Voigt} transformation is specific for the fit region; use of a fit region other than that for which the transformation is specified results in the errors indicated in the insert to Fig. 2. The transformation for the doublet differs from that of the singlet. The coefficients defined as for the singlet are shown in Table 3.

Linewidth/Splitting Ratio Dependence of Fit Fidelity

The fidelity of the doublet sum-function parameters to those of the Voigt depends on the ratio of the peak-to-peak linewidth to the splitting. Table 4 shows the maximum deviation of sum-function fit parameters from the Voigt parameters with a fit region of the splitting plus four linewidths for different linewidth-to-splitting ratios. With peak-to-peak linewidth-to-splitting ratios of 2/3 and 1, the quantitative results were virtually identical. At a peak-to-peak linewidth-to-splitting ratio of 1, the central trough peak feature was no longer visible (R = 0) (data not shown). Nonetheless, for the fitting of the sum function to the Voigt doublet, the lines appeared well decoupled by the fitting. As can be seen in Table 4, for larger peak-to-peak linewidth-to-splitting ratios, the fitting fidelity deteriorated rapidly.

Fitting a Noisy Voigt Doublet

The moderately noisy synthetic spectrum in Fig. 1 (Voigt + Gaussian noise, σ = 2.5% V_{pp}) is shown with a sum-func-

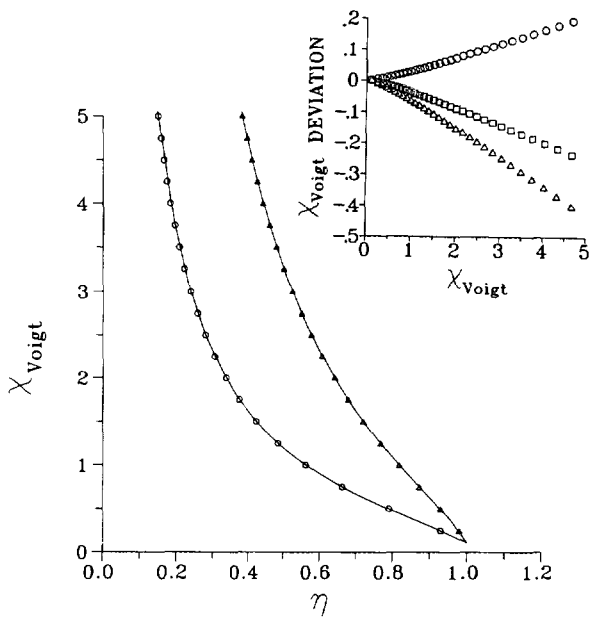

FIG. 2. Plot of the input Gaussian/Lorentzian linewidth ratio of the Voigt singlet, χ_{Voigt}, vs the sum-function weight parameter, η, derived from the sum-function fit to the Voigt. △, χ_{Voigt} vs η_A, the area-normalized sum-function Lorentzian weight parameter; ○, χ_{Voigt} vs η_H, the height-normalized sum-function Lorentzian weight parameter. The fit region is four peak-to-peak linewidths. The interpolating lines are fits to Eq. [8] with the parameters given in Table 3. (Insert) The change in χ_{Voigt} at a given value of η induced by a change in the fit region from the χ_{Voigt} evaluated with a reference fit region of four linewidths. ○, −0.8 linewidths; □, +1 linewidth; △, +3 linewidths. For a shift of the fit region by one linewidth from four, there is a shift in the χ_{Voigt} (and potential misassignment) of approximately 5%.

TABLE 3

Coefficients for the η–χ_{Voigt} Transformation Indicated in the Equation [Eq. (8)] $\chi_{Voigt} = (a\eta^2 + b\eta + c)/(\eta^2 + d\eta + e)$ for Various Fit Regions, Defined in Units of Peak-to-Peak Voigt Linewidths

Fit normalization	Line type	Fit region	a	b	c	d	e
Area	Singlet	3.2	−2.49082	5.68959	−3.20739	−1.07298	−0.00460
		4.0	−2.35775	5.42045	−3.07144	−1.0748	−0.00465
		5.0	−2.19226	5.09119	−2.90817	−1.07901	−0.00449
		7.0	−2.07936	4.86226	−2.79250	−1.08176	−0.00407
	Doublet	3.2	−2.26353	5.24725	−2.99338	−1.08211	−0.00514
		4.0	−2.11240	4.95808	−2.85612	−1.08806	−0.00481
		5.0	−1.95763	4.64381	−2.69693	−1.09142	−0.00463
		7.0	−1.83688	4.40630	−2.58095	−1.09780	−0.00353
Height	Singlet	3.2	−0.26625	1.36127	−1.13317	−1.34042	−0.00150
		4.0	−0.23627	1.28380	−1.08474	−1.33738	−0.00201
		5.0	−0.16482	1.17093	−1.04828	−1.37594	−0.00137
		7.0	−0.13915	1.10447	−1.00719	−1.37573	−0.00163
	Doublet	3.2	−0.4317	1.3730	−0.9486	−1.1187	−0.0112
		4.0	−0.3808	1.2814	−0.9084	−1.1269	−0.0110
		5.0	−0.3289	1.1809	−0.8601	−1.1346	−0.0105
		7.0	−0.2937	1.1089	−0.8236	−1.1389	−0.0099

Note. Fit-region changes induced a 5% change in the χ_{Voigt} per linewidth change in the fit region. The coefficients for the η–χ_{Voigt} transformation for the doublet are also presented. The doublet, which was the principal focus of the spectral modeling, had a linewidth/splitting ratio = 2/3. The difference between the doublet and singlet η–χ_{Voigt} transformations is roughly that of singlet transformations differing in fit regions by two linewidths.

tion fit. Table 5 summarizes the results obtained with the area-normalized sum function to fit the Voigt doublet (peak-to-peak linewidth/splitting = 2/3) to which 100 sets of 2.5% noise were added. The results are given for a fit region of four linewidths plus the splitting, but they were essentially the same for fit regions of the splitting plus three to seven linewidths. The deviations of the mean from the zero noise deviation were comparable to the standard deviation of the mean. Thus, no bias was introduced into the fits by Gaussian noise. The population standard deviations for parameters intrinsic to the spectral shape (e.g., height or linewidth) were

TABLE 4

Percentage Deviation of Various Parameters Extracted from the Sum Function from the "Exact" or Input Values from the Voigt Tabulated for Different Linewidth (ΔB)-to-splitting (A) Ratios

$\Delta B/A$	Linewidth discrepancy (%) (χ)	Splitting discrepancy (%) (χ)	Height discrepancy (%) (χ)
2/3	0.2 (3)	0.25 (1)	0.6 (1)
1	0.2 (1, 3)	0.1 (1, 3)	0.4 (1)
2	2.6 (1)	2.5 (1, 3)	0.7 (1)
4	3 (1)	22 (1, 3)	0.7 (1)

Note. $\Delta B/A$ less than 2/3 was not considered insofar as the similarity of the doublet result to the singlet result indicates the fitting procedure to have decoupled the lines adequately. The deviations were evaluated with a fit region of 4 linewidths plus the splitting. Other fit regions (3, 3.2, 5, and 7 linewidths plus the splitting) gave nearly identical results. The numbers are the maximum among a set of Voigt profiles with χ_{Voigt} = 0.25, 0.5, 1.0, and 3.0. The χ_{Voigt}, in parentheses, of maximum deviation is indicated.

TABLE 5

Characteristics of the Distributions of Fit Parameters from Fits to a Voigt Profile to Which 100 Sets of 2.5% Noise, as Defined in the Text, Were Added

	Mean value − zero noise value (% deviation)	Estimated population standard deviation (%)
ΔB^0_{pp}	0.012	0.17
Splitting	0.005	0.04
Height	0.03	0.12
R value	0.04	0.24
ΔB^L_{pp}	0.03	1.5
ΔB^G_{pp}	0.15	4.2

Note. The values are the maximum among fits performed with a set of χ_{Voigt} = 0.25, 0.5, 1.0, and 3.0 and a fit region = 4.0 linewidths plus the splitting. Other fit regions gave similar numbers. Note that the standard deviation of the mean in each case is 1/10th the standard deviation. The similarity of these standard deviations of the mean to the difference between the zero noise fit parameters and the mean value of the parameters extracted from the noisy spectra indicates that the Gaussian noise has not biased the mean.

more than an order of magnitude smaller than the noise standard deviation. The fits to the Lorentzian and Gaussian components of the Voigt when the η–χ_{Voigt} transformation was used were "noisier" than intrinsic shape parameters due to the nonorthogonality of the component functions.

Fitting Data

Figure 3A shows the results of a typical fit of the area-normalized sum function to a low-noise ($\sigma_{noise} \sim 0.5\%$) spectrum from the central nitrogen manifold of a 100 μM nitrogen-equilibrated sample of mHCTPO. Figure 3B shows the residuals. It is difficult to discern any systematic variation. Both normalizations (area and height) gave identical linewidths, line spacings, and line heights.

In Fig. 4 the Lorentzian linewidth is plotted as a function of oxygen concentration for six spin-label concentrations from 0.05 to 1 mM. The expected linearity of the response is verified. The slope is 550 ± 13 mG/mM. Also plotted in Fig. 4 are data from the work by Hyde and Subczynski at 0.1 mM and 10 GHz; they measured the linewidth of the individual hydrogen lines in fully protonated CTPO (*22*). This is a direct measure of the Lorentzian component. There

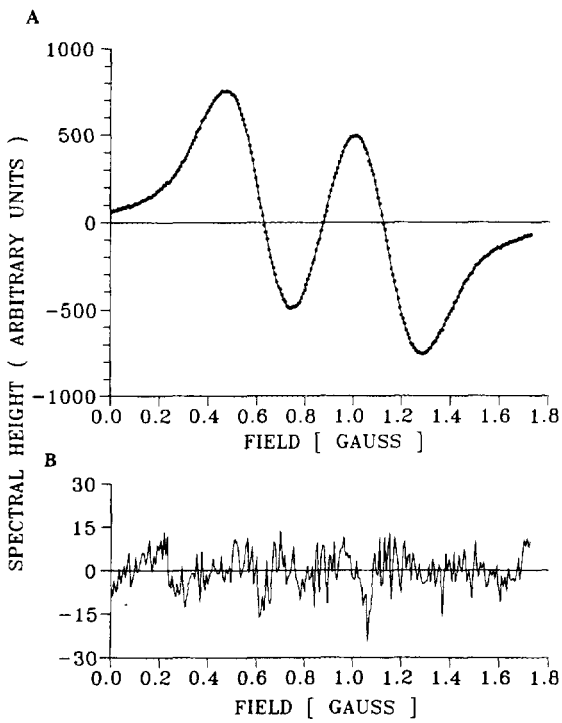

FIG. 3. (A) Fit of the sum function to the central doublet of mHCTPO, 4-hydro-3-carbamoyltetraperdeuteromethyl-3-pyrrolinyl-1-oxy. Data-acquisition conditions are described in the text. The fit was performed in two passes, with a final pass having a fit region of the splitting plus four linewidths which occupies nearly the entire window displayed. (B) Residuals (data minus fit). The spectral-noise standard deviation is approximately 0.5% of the V_{pp}, or about one-fifth that used for the noisy Voigt simulations.

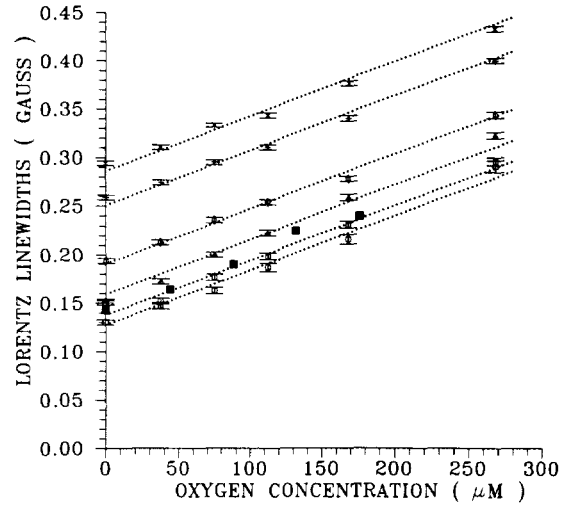

FIG. 4. Lorentzian linewidth of the central doublet lines of mHCTPO vs molecular oxygen concentration for different concentrations of mHCTPO. Oxygen concentration is derived from a Henry's law constant of 12.5 μM/% (1.64 μM/mm) in resonator room-temperature (27°C) water (*43*). The Lorentzian (spin-packet) linewidth is extracted from the sum-function fits over a fit region of the splitting plus four linewidths in a two-pass fit. Also shown is a set of lines (· · ·) fitted to the data with the hypothesis of identical slopes as a function of oxygen concentration, but a different intercept for each spin-label concentration. The common slope is 550 ± 13 mG/mM. The individual point uncertainties and slope uncertainties were derived as described in the text; they are measures of random noise only. The direct measurement of the Lorentzian (spin-packet) component at 37°C by Hyde and Subczynski (*22*) (■) is also shown uncorrected for temperature. Measurements (data not shown) indicate that the correction for temperature is less than 10 mG. ○, 50 μM; □, 100 μM; ■, 100 μM; △, 200 μM; ◇, 400 μM; +, 750 μM; ×, 1000 μM.

is very good agreement with the measurements presented here. The Lorentzian linewidth is plotted vs spin-label concentration at various equilibrating gas oxygen mole fractions in Fig. 5. A linear relationship is seen, with a slope of 167 ± 3 mG/mM that is independent of the oxygen concentration.

In Fig. 6, the hyperfine coupling vs concentration, fitted at six spin-label concentrations, is plotted from 0.05 to 1 mM. Each point represents a total of 12 measurements taken from samples equilibrated with N_2/O_2 gas at six O_2 fractions ranging from less than 0.1 to 21.5%. The error bars indicated are the standard errors of the means of measurements taken with the entire set of oxygen concentrations. These error bars are typically 0.3 mG. The coupling diminished linearly from an extrapolated zero concentration value of 518 ± 2 mG with a slope of −27 ± 2 mG/mM (errors include a systematic allowance), with a 5% change over the range of concentrations used. Despite the small fractional size of this effect, it is two orders of magnitude larger than the effect of oxygen on the coupling. The insensitivity of line splitting to oxygen has been noted previously (*23*). The linear dependence on spin-label concentration of the spin-exchange-in-

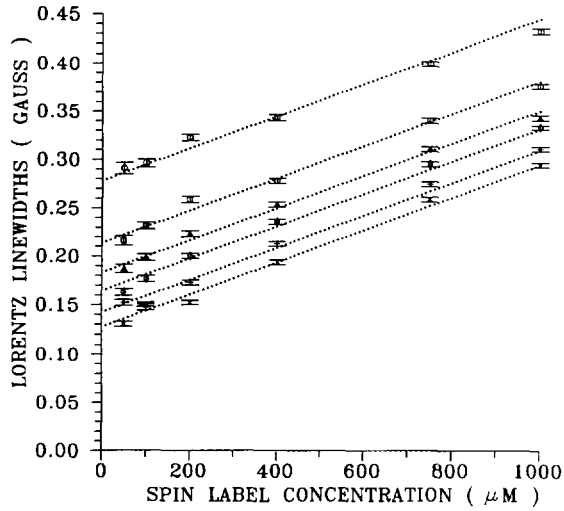

FIG. 5. Lorentzian (spin-packet) linewidth of central doublet line of mHCTPO vs concentration of mHCTPO for different mole fractions of oxygen in the equilibrating gas. The fitting conditions are as described in the legend to Fig. 4. Also shown are lines fitted to the data with the hypothesis of identical slopes, but different intercepts for each oxygen mole fraction. The common slope is 167 ± 3 mG/mM. Uncertainties are as described in the text. ○, 21.5% O_2; □, 13.5% O_2; △, 9% O_2; ◇, 6% O_2; +, 3% O_2; ×, 0% O_2.

duced line-splitting collapse has been discussed previously (*24*). This allows an intrinsic spectral feature sensitive to the *local* spin-label concentration to distinguish self-broadening effects from those due to oxygen. The concentration dependence of the Gaussian linewidth from the mHCTPO was constant as a function both of spin label (50 to 1000 μM) and of oxygen (less than 1 to 250 μM) concentrations to within ±10 mG (data not shown) with a value of 220 mG.

DISCUSSION

In this work, we investigate the use of an easily evaluated analytic shape, the Lorentzian/Gaussian sum function which was chosen because it fits spectral lines well. Fitting this shape to spectra was used to extract basic parameters of two kinds: intrinsic lineshape measures—overall linewidth, line position, height, and spectral feature height ratios—and model-dependent line components—Voigt Lorentzian and Gaussian components. The process focuses the full information in the spectrum on the spectral parameters. The positions of data points on the rising and falling portions of the spectrum are more sensitive to slight variations of the line positions and linewidths than are those in the peaks and troughs where the width is most commonly defined (*25*). Fitting to a spectral-shape hypothesis allows these points to be included in the definition of linewidth and line position. The definition of the splittings of overlapping lines is also complicated in the absence of some spectral-shape hypothesis.

The spectral fitting may be used to reduce noise. An adequate fit hypothesis provides substantial a priori coordinating information. In the noisy Voigt simulation, both the fitted height and the splitting have population standard deviations that are reduced by more than an order of magnitude relative to the point standard deviation. When compared with earlier measurements of line splitting (*4*), the current measurements are nearly an order of magnitude more accurate. The error matrix from the algorithm provides a convenient estimate of the uncertainties in the fit parameters. This is invaluable for determining whether parameter variation is statistical or systematic.

This technique is rapid relative to evaluation of full convolution, less affected by noise than the Fourier transform (*26–28*), more compact than table look-up strategies (*9*), and less baseline sensitive than moment analyses (*29*). An algorithm that approximates the Voigt (*30*) may constitute a possible alternative to the sum function. In circumstances where array interrogation will not easily provide initial parameters, other strategies may be necessary (*26, 31–33*).

Other minimization algorithms are available (*34, 35*). The least-squares criterion may not be the optimum criterion for judging goodness of fit (*36–40*). The derivative Voigt shape is not necessarily the best by which to characterize EPR lineshapes. However, they are familiar and give a good fit to spectral data. The investigation of larger numbers of over-

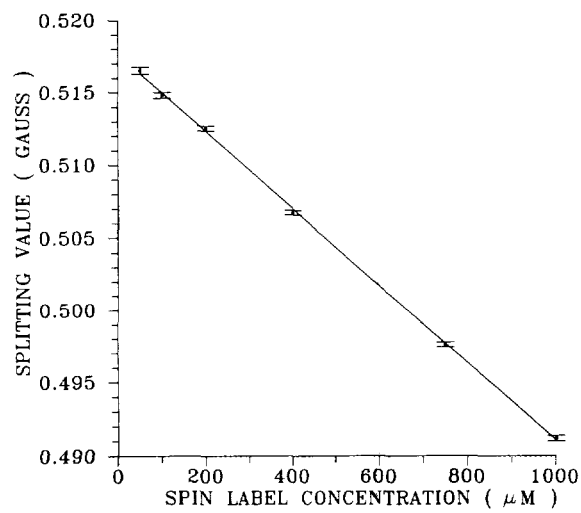

FIG. 6. Hyperfine splitting of the central doublet of mHCTPO vs mHCTPO concentration for all oxygen concentrations. Each point represents the average of splittings evaluated from spectra taken from solutions equilibrated with various mole fractions of oxygen: 0, 3, 6, 9, 13.5, and 21.5%. The point uncertainties indicated represent the standard deviation of the mean of these values; they are consistent with the errors propagated from the spectra as described in the text. Addition of oxygen dependence neglibly diminishes the χ^2 value per degree of freedom of the fit. The fit slope is 26.5 ± 0.2 mG/mM, the intercept is 517.6 ± 0.2 mG, and the uncertainties were obtained as described in the text. These uncertainties are consistent with the hypothesis of no oxygen dependence. The numbers quoted in the text include estimates of the systematic uncertainty.

lapping lines is incomplete; the large fit-region fit fidelity indicated in the tables provides a worst-case estimate. The effects of saturation, overmodulation, and spectral passage for times small enough to affect the spectral symmetry have yet to be investigated. The inclusion of a dispersive component is straightforward (*41*); an artifact of symmetry opposite to that of the spectrum has little effect on the extracted parameters (proof not shown).

In summary, we have developed a rapid and accurate method by which to fit EPR spectra and with which to unfold the Lorentzian and Gaussian components. This method has been used to extract spectral parameters from EPR spectra with noise. In the context of EPR *in vivo* (*42*), it provides the possibility of relatively accurate spectral analysis. In a more general context, it allows an increase in sensitivity, for some spectral parameters, by an order of magnitude.

APPENDIX

This Appendix is devoted to a brief derivation of the transformation between the Lorentzian weight parameter for the sum function normalized to unit peak-to-peak height, η_H, and the Lorentzian weight parameter for the sum function normalized to unit doubly integrated intensity, η_A. Both sum functions are fitted to the same data with peak-to-peak height V_{pp} and doubly integrated intensity A. Equations [5] and [6] are rewritten as

$$F_H(x) = V_{pp}[\eta_H c_L^H L(x) + (1 - \eta_H) c_G^H G(x)]$$

$$F_A(x) = A[\eta_A c_L^A L(x) + (1 - \eta_A) c_G^A G(x)],$$

where the individual term normalizations are

$$c_L^H = 8, \quad c_G^H = e^{1/2}/2, \quad c_L^A = 8(3)^{1/2}/[\pi(\Delta B_{pp}^0)^2],$$

$$c_G^A = 4/[(2\pi)^{1/2}(\Delta B_{pp}^0)^2],$$

and the functions are

$$L(x) = x/(3 + x^2)^2 \quad \text{and} \quad G(x) = x \exp(-x^2/2).$$

The conditions that

$$F_A(1) = V_{pp}/2$$

and

$$\int\int dB^2 F_H[x(B)] = A$$

may be used to eliminate the normalization constants (V_{pp} and A), leaving a relationship between the Lorentzian weight parameters and the ratios of the individual term normalizations,

$$r_L = c_L^A/c_L^H \quad \text{and} \quad r_G = c_G^A/c_G^H,$$

such that $[\eta_H/r_L + (1 - \eta_H)/r_G](\eta_A r_L + (1 - \eta_A) r_G] = 1$, giving

$$\eta_H = r_L \eta_A/[\eta_A r_L + (1 - \eta_A) r_G]$$

and

$$\eta_A = r_G \eta_H/[\eta_H r_G + (1 - \eta_H) r_L].$$

ACKNOWLEDGMENTS

We thank Michael K. Bowman for useful criticism and comments. This work was supported by American Cancer Society Research Grant PDT-262, NIH Research Grant CA 50679, and U.S. Army Research Office Grant DAALO 3-88-k-0006.

REFERENCES

1. W. Voigt and S. B. Bayer, *Acad. Wiss.*, 603 (1912).
2. M. W. P. Strandberg, *Ann. Phys.* **77,** 174 (1973).
3. G. K. Wertheim, M. A. Butler, K. W. West, and D. N. E. Buchanan, *Rev. Sci. Instrum.* **45,** 1369 (1974).
4. B. L. Bales, L. J. Berliner, and J. Reuben (Eds.), "Biological Magnetic Resonance," Vol. 8, p. 77, Plenum, New York, 1989.
5. B. L. Bales, *J. Magn. Reson.* **38,** 193 (1980).
6. B. L. Bales, *J. Magn. Reson.* **48,** 418 (1982).
7. M. W. Zemansky, *Phys. Rev.* **36,** 219 (1930).
8. T. G. Castner, *Phys. Rev.* **115,** 1506 (1959).
9. D. W. Poesner, *Aust. J. Phys.* **12,** 184 (1959).
10. S. N. Dobryakov and Ya. S. Lebedev, *Sov. Phys. Dokl.* **13,** 873 (1969).
11. W. H. Press, B. P. Flannery, S. A. Teukolsky, and W. T. Vetterling, "Numerical Recipes: The Art of Scientific Computing," p. 523, Cambridge Univ. Press. Cambridge, 1986.
12. W. H. Press, B. P. Flannery, S. A. Teukolsky, and W. T. Vetterling, "Numerical Recipes: The Art of Scientific Computing," p. 202, Cambridge Univ. Press, Cambridge, 1986.
13. H. J. Halpern, M. Peric, T-D. Nguyen, D. P. Spencer, B. D. Teicher, B. D., Y. J. Lin, and M. K. Bowman, *J. Magn. Reson.* **90,** 40 (1990).
14. Y. J. Lin, B. A. Teicher, and H. J. Halpern. *Labelled Comps. Radiopharm.* **28,** 621 (1990).
15. B. L. Bales, R. A. Blum, D. Mareno, M. Peric, and H. J. Halpern. *J. Magn. Reson.* **98,** 299 (1992).
16. H. J. Halpern, D. P. Spencer, J. van Polen, M. K. Bowman, A. C. Nelson, E. M. Dowey, and B. A. Teicher, *Rev. Sci. Instrum.* **60,** 1040 (1989).
17. M. K. Bowman, T. J. Michalski, M. Peric, and H. J. Halpern, *Pure Appl. Chem.* **62,** 271 (1990).
18. W. H. Press, B. P. Flannery, S. A. Teukolsky, and W. T. Vetterling, "Numerical Recipes: The Art of Scientific Computing," p. 529, Cambridge Univ. Press, Cambridge, 1986.
19. P. R. Bevington, "Data Reduction and Error Analysis for the Physical Sciences," p. 235, McGraw-Hill, New York, 1969.
20. P. R. Bevington, "Data Reduction and Error Analysis for the Physical Sciences," p. 56, McGraw-Hill, New York, 1969.
21. P. R. Bevington, "Data Reduction and Error Analysis for the Physical Sciences," p. 69, McGraw-Hill, New York, 1969.

22. J. S. Hyde and W. K. Subczynski, *J. Magn. Reson.* **56,** 125 (1984).
23. M. T. Jones, *J. Chem. Phys.* **38,** 2892 (1963).
24. Yu M. Molin, K. M. Salikov, and K. I. Zamaraev, "Spin Exchange: Principles and Applications in Chemistry and Biology," p. 112, Springer-Verlag, Berlin, 1980.
25. C. P. Poole, "Electron Spin Resonance: A Comprehensive Treatise on Experimental Techniques," pp. 775–784, Wiley, New York, 1967.
26. P. J. Hore, *J. Magn. Reson.* **62,** 561 (1985).
27. K. Ramani, S. Ganapathy, and R. Srinivasan, *J. Magn. Reson.* **24,** 231 (1976).
28. S. J. Nelson and T. R. Brown, *J. Magn. Reson.* **75,** 229 (1987).
29. H. A. Farach and H. Teittelbaum, *Can. J. Phys.* **45,** 2913 (1967).
30. A. Cabral-Prieto, H. Jimenez-Dominguez, L. Gonzalez-Tovany, S. Galindo, H. Flores-Llamas, and Torres-Valderrama, *J. Magn. Reson.* **89,** 568 (1990).
31. R. A. Jackson, *J. Magn. Reson.* **75,** 174 (1987).
32. I. Heynderickx, H. DeRaedt, and D. Schoemaker, *J. Magn. Reson.* **70,** 134 (1986).
33. R. E. Hoffman and G. C. Levy, *J. Magn. Reson.* **83,** 411 (1989).
34. W. H. Press, B. P. Flannery, S. A. Teukolsky, and W. T. Vetterling, "Numerical Recipes: The Art of Scientific Computing," p. 289, Cambridge Univ. Press, Cambridge, 1986.
35. W. H. Press, B. P. Flannery, S. A. Teukolsky, and W. T. Vetterling, "Numerical Recipes: The Art of Scientific Computing," p. 294, Cambridge Univ. Press, Cambridge, 1986.
36. N. P. Archer, W. V. Prestwich, and G. L. Keech, *Nuclear Instrum. Methods* **44,** 114 (1966).
37. I. B. C. Matheson, *Comput. Chem.* **14,** 49 (1990).
38. J. S. Hyde, M. Pasenkiewica-Gierula, R. Basosi, W. Froncisz, and W. E. Antholine, *J. Magn. Reson.* **82,** 63 (1989).
39. P. J. Huber, "Robust Statistics," Wiley, New York, 1981.
40. K. L. Lange, R. J. A. Little, and J. M. G. Taylor, *J. Am. Stat. Assoc.* **84,** 881 (1989).
41. G. Pake and E. M. Purcell, *Phys. Rev.* **74,** 1184 (1948).
42. H. J. Halpern, M. Peric, and T.-D. Nguyen, *Phys. Med.* **7,** 45 (1991).
43. C. D. Hodgeman, R. C. Weast, and S. M. Selby, "Handbook of Chemistry and Physics," 42nd ed., p. 1708, Chemical Rubber Publishing, Cleveland, 1960.